The Astrophysical Journal Letters, 876:L21 (6pp), 2019 May 10 https://doi.org/10.3847/2041-8213/ab1b4f

Effect of the Interstellar Magnetic Field Draping around the Heliopause on the *IBEX* Ribbon

Konstantin V. Gamayunov[1], Jacob Heerikhuisen[2,3], and Hamid K. Rassoul[1]
[1] Department of Aerospace, Physics and Space Sciences, Florida Institute of Technology, Melbourne, FL 32901, USA; kgamayunov@fit.edu
[2] Department of Space Science, University of Alabama in Huntsville, Huntsville, AL 35899, USA
[3] Center for Space Plasma and Aeronomic Research, University of Alabama in Huntsville, Huntsville, AL 35899, USA
Received 2019 March 7; revised 2019 April 15; accepted 2019 April 22; published 2019 May 6

Abstract

A dominant feature in all-sky maps of energetic neutral atoms (ENAs) from NASA's *Interstellar Boundary EXplorer* (*IBEX*) is a ribbon of enhanced fluxes. This ribbon was not predicted before *IBEX*, but all the up-to-date *IBEX* observations support a secondary ENA mechanism for the ribbon formation. There are two different classes of the secondary ENA model; the first class assumes a weak pitch angle scattering of energetic protons in the local interstellar medium (LISM), and the second class assumes strong, but spatially localized, scattering. A recent work by Gamayunov et al. strongly supports a "weak scattering" version, and here we extend the scope of the Gamayunov et al. model by using a more realistic interstellar magnetic field (ISMF) from our global MHD-plasma/kinetic-neutral simulation of the heliosphere–LISM interaction in place of the simple analytical model used previously. The main conclusions of our analysis are summarized as follows. (1) Pitch angle scattering of energetic protons in the LISM is not the primary mechanism that controls the width of ribbon. Instead, the ribbon width is mainly determined by draping of the ISMF around the heliopause. (2) The intensity of the ribbon is controlled by pitch angle scattering of energetic protons in the LISM. A model–*IBEX* comparison suggests that generation of the small-scale local turbulence is suppressed in the LISM. On the other hand, the large-scale interstellar turbulence (LSIT) alone or an interplay between the LSIT and the case of no scattering leads to a good agreement between the model and *IBEX* fluxes.

Key words: ISM: kinematics and dynamics – ISM: magnetic fields – plasmas – scattering – solar wind – turbulence

1. Introduction

NASA's *Interstellar Boundary EXplorer* (*IBEX*) spacecraft is imaging energetic neutral atoms (ENAs) propagating to Earth from the outer heliosphere and the local interstellar medium (LISM). A dominant feature in all ENA maps is a ribbon of enhanced fluxes that was not predicted before *IBEX*. While more than a dozen models of the ribbon formation were proposed (e.g., McComas et al. 2009, 2011, 2014b; Isenberg 2014; Giacalone & Jokipii 2015), all the up-to-date *IBEX* observations strongly support a secondary ENA mechanism for the ribbon formation. Based on this fact, McComas et al. (2017) suggested to adopt a secondary ENA mechanism as a nominal explanation of the *IBEX* ribbon. The secondary ENA mechanism is based on the fact that an average solar wind (SW) velocity inside the termination shock and in the inner heliosheath (IHS) is anti-sunward. So, after charge-exchange between the SW/IHS protons and interstellar H, a majority of primary ENAs propagates away from the Sun, and a large fraction of them reaches the LISM. ENAs in the LISM experience charge-exchange again creating energetic protons. These protons propagate along an inhomogeneous interstellar magnetic field (ISMF), convect together with the LISM flow in the direction perpendicular to magnetic field, experience a pitch angle scattering by waves, and finally, after characteristic charge-exchange time in the LISM, charge-exchange with the cold interstellar H creating secondary ENAs. Then, a sunward-propagating fraction of the secondary ENAs can be detected by *IBEX*. Following the paper by Heerikhuisen et al. (2010), an outlined mechanism of the ribbon formation is called the "secondary ENA" mechanism, and a schematic of this mechanism is shown in Figure 1 of the paper by McComas et al. (2010).

There are two qualitatively different classes of the secondary ENA models. The first class assumes a weak pitch angle scattering of energetic pickup protons in the LISM (e.g., Gamayunov et al. 2010; Heerikhuisen et al. 2010), and the second class assumes strong, but spatially localized, scattering of pickup protons in the LISM (e.g., Schwadron & McComas 2013; Isenberg 2014). Recently, Gamayunov et al. (2017, hereafter Paper I) presented a test of the "weak scattering" version of the secondary ENA model using their gyro-averaged kinetic model for the evolution of the phase space distribution of energetic protons in the LISM. As an input for their test, they used distributions of the primary ENAs from 3D MHD-plasma/kinetic-neutral model of the heliosphere–LISM interaction (Pogorelov et al. 2004; Heerikhuisen et al. 2005, 2016; Heerikhuisen & Pogorelov 2010). In addition, the magnetic field spectrum for the large-scale interstellar turbulence (LSIT) and an upper limit for the amplitude of small-scale local turbulence (SSLT) generated by pickup protons were taken from observations by *Voyager 1* in the LISM (Burlaga et al. 2014, 2015). The results of hybrid simulations of energetic protons were also used to set the bounding wavenumbers for the spectrum of SSLT. The test results presented in Paper I strongly support the "weak scattering" version of the secondary ENA model. However, Paper I used an oversimplified analytical model for the ISMF. While the analytical model used represented a reasonable approximation for the purposes of initial test in Paper I, a more realistic magnetic field from the global MHD-plasma/kinetic-neutral model of the heliosphere–LISM interaction has a more realistic magnetic field draping around the heliopause (HP). This realistic draping broadens an

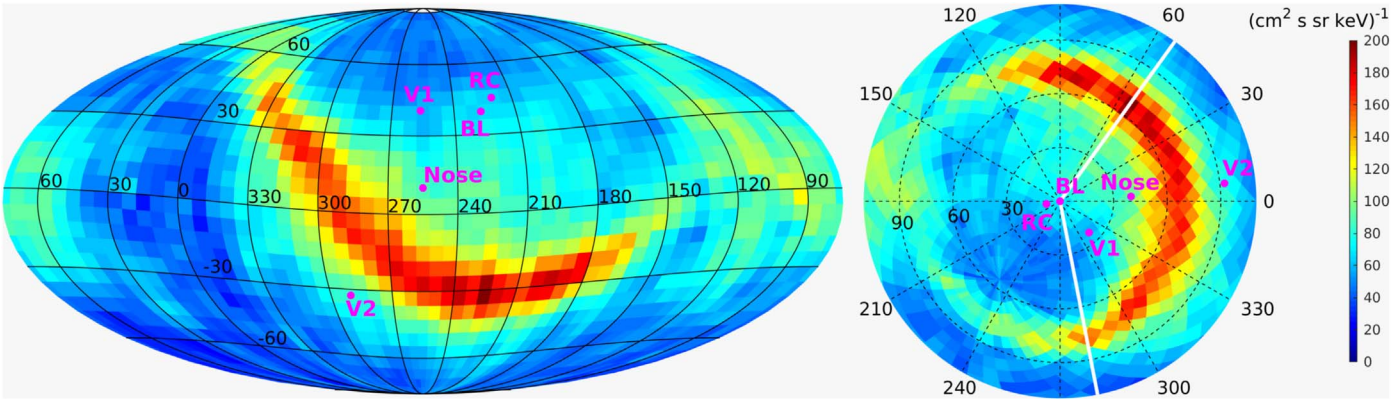

Figure 1. The *IBEX* first five-year averaged ENA flux for 1.11 keV. (Left) The full-sky map in Mollweide projection, where the grid lines are in ecliptic coordinates J2000. The directions to the *Voyager 1* and *2* spacecraft are indicated by *V1* and *V2*, along with the direction from which interstellar medium flow originates (Nose) at (long., lat.) = (255°, 5°), the observed ribbon center (RC) at (long., lat.) = (220.°3, 40.°5), and the direction of pristine ISMF (BL) at (long., lat.) = (227°, 34.°8) used in our global MHD-plasma/kinetic-neutral model of the heliosphere–LISM interaction. (Right) The polar plot of ENA flux centered on BL that is produced from the left map using the transformation introduced by Funsten et al. (2013). Note that in order to align our coordinate axis $\theta = 0°$ in the same way Funsten et al. did, we used the nose direction (long., lat.) = (259°, 5°) from the Funsten et al. paper, but nose direction indicated here is an updated direction from the paper by McComas et al. (2015). The two white lines show the cuts through the azimuthal angles $\theta = 54°$ and $\theta = 281°$.

ENA flux profile around ribbon peak, and so potentially affects the results presented in Paper I.

Here we extend the scope of Paper I by using ISMF from our global MHD-plasma/kinetic-neutral model of the heliosphere–LISM interaction instead of a simple analytical model used in Paper I. We are confident that our global MHD-plasma/kinetic-neutral model gives a reasonable approximation for the shape of HP and the draping of ISMF around the HP because (1) the distances to the HP in the *Voyager 1* and *2* directions in the simulation match the observed crossing distances to within a few astronomical units, (2) the properties of ribbon obtained using a simpler ribbon model match those observed by *IBEX* (Zirnstein et al. 2016), and (3) in the same Zirnstein et al. paper we show in Table 2 that the draped magnetic field in the simulation is close to that observed by *Voyager 1*. Except the above replacement for the ISMF model, all the other input parameters for our modeling presented here are the same as in Paper I, where a detailed model description and specification can be found. As in Paper I, here we also purposely turn off an ENA production in the IHS in order to focus solely on our model of ribbon. The model ribbon flux can then be compared directly to the observed ribbon flux once the diffuse globally distributed flux (GDF) has been subtracted out. The model flux from IHS could be added to our model ribbon flux presented here. However, as the IHS fluxes are modeled differently in the framework of our global MHD-plasma/kinetic-neutral model, it would mean comparing ENA data to the conflation of two models, which we feel would be more problematic to interpret. Also, here we analyze only two azimuthal cuts, through $\theta = 51°$ and $\theta = 282°$, as it was done in Paper I.

2. Results

The direction to ribbon center (RC) is not aligned with the direction of pristine ISMF in the LISM (e.g., Zirnstein et al. 2016 and references therein). The vector of pristine ISMF is offset from RC by ~8° toward the nose direction (the direction from which interstellar medium flow originates), and these three vectors (the vectors to RC and nose, and ISMF) belong to a plane (Zirnstein et al. 2016). In our initial analysis presented in Paper I we used the azimuthal angles θ that refer to the polar coordinates centered on RC (see the right panel in Figure 1 of Paper I). Here, however, we use the polar coordinates centered on the direction of pristine ISMF in the LISM (BL) used in our global MHD-plasma/kinetic-neutral model of the heliosphere–LISM interaction. So, first, we transform the *IBEX* observations into the polar coordinates centered on BL. Figure 1 shows the average ENA flux at 1.11 keV from the seventh *IBEX* data release (McComas et al. 2014a), where the two representations of the all-sky map are shown. The left panel in Figure 1 is nearly identical to the left panel in Figure 1 of Paper I, except the direction to BL is added here. The right panel in Figure 1 shows a polar plot of the *IBEX* ENA flux, but in contrast to Paper I the polar coordinates here are centered on BL. In Paper I we analyzed the two azimuthal cuts, through $\theta = 51°$ and $\theta = 282°$, where the polar coordinates were centered on RC. The ecliptic coordinates of ribbon maximum in the former cut are (long., lat.) = (224.°7, −32.°7), whereas in the latter cut the coordinates of maximum are (long., lat.) = (326.°5, 43°). The two azimuthal cuts through the above two ribbon maxima in the polar coordinates centered on BL give the new angles $\theta = 54°$ and $\theta = 281°$, which are shown by the two white lines in the right panel of Figure 1, and these two cuts will be analyzed below.

2.1. Azimuthal Cut through θ = 54°

Figure 2 shows ISMF in the azimuthal cut through $\theta = 54°$. (Note that only region $y \geqslant 0$ is shown here because the region $y < 0$ corresponds to the azimuthal cut through $\theta = 54° + 180° = 234°$.) The shown ISMF is obtained from our global MHD-plasma/kinetic-neutral model of the heliosphere–LISM interaction (Pogorelov et al. 2004; Heerikhuisen et al. 2005, 2016; Heerikhuisen & Pogorelov 2010), where ISMF at infinity is set to 3 μG, and the nose and BL directions are shown in Figure 1 (Heerikhuisen et al. 2014). The magenta line in Figure 2 shows the heliopause location. The location of heliopause is determined by the plasma temperature contour $T = 50{,}000$ K. For the front of heliosphere the temperature drops sharply across the heliopause from ~1,000,000 K inside the heliosphere down to ~25,000 K just outside the heliosphere. Toward the tail of heliosphere, the simulated heliopause is less sharply defined due to the increased size of grid cells and also cooling of the SW plasma as it convects through the

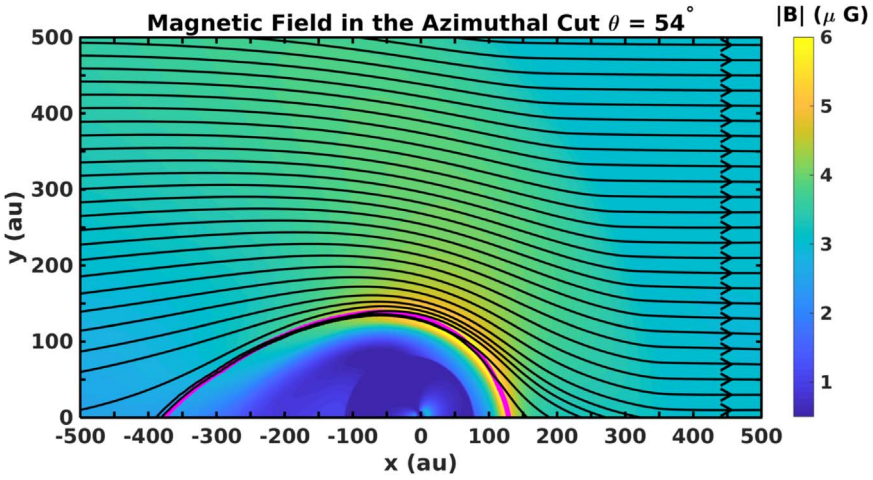

Figure 2. ISMF in the azimuthal cut $\theta = 54°$ that is obtained from the global MHD-plasma/kinetic-neutral model of the heliosphere–LISM interaction, where the nose and BL directions are shown in Figure 1, and ISMF at infinity is set to 3 μG. The x-axis is directed along ISMF at infinity, and the y-axis has an azimuthal angle $\theta = 54°$. The magenta line shows the heliopause location and the black lines show projection of the ISMF lines into the plane $\theta = 54°$, where the magnetic field directions are indicated by arrows. The background color shows a total amplitude of ISMF, including the magnetic field component perpendicular to the plane $\theta = 54°$, according to the color bar on the right side of the figure.

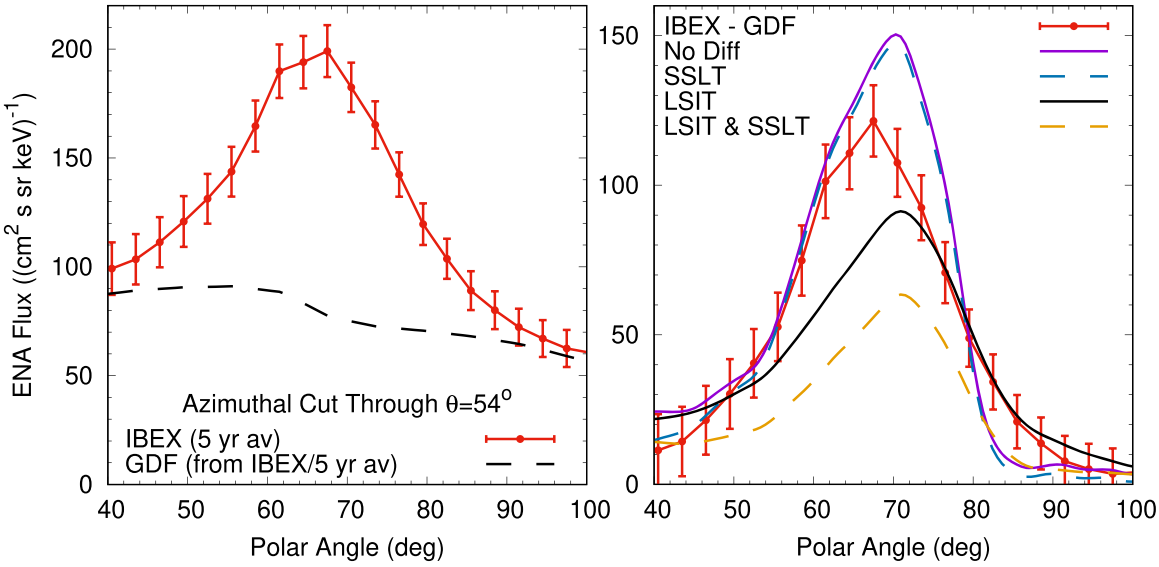

Figure 3. The 1.11 keV ENA fluxes at the Sun/*IBEX* location vs. polar angle in the azimuthal cut $\theta = 54°$. (Left) *IBEX* (5 yr av) is the *IBEX* first five-year averaged ENA flux, which is shown by the red line. The error bars show $\pm 3\sigma$, where σ is the standard deviation reported for the *IBEX* data. The diffuse globally distributed flux (GDF) separated from the *IBEX* first five-year averaged ENA flux is shown by the black dashed line. (Right) "*IBEX*–GDF" is the observed "pure ribbon" flux, which is a difference between the *IBEX* and GDF fluxes shown in the left panel, and error bars show the same $\pm 3\sigma$ for the *IBEX* data. The four model profiles are shown for the cases of no pitch angle diffusion of energetic protons in the LISM (No Diff), diffusion due to the SSLT only, LSIT only, and composite LSIT & SSLT. (Note that in Figure 7 of Paper I we have mistakenly used the data variance instead of standard deviation to plot the error bars.)

heliosphere. Our extensive experience shows that the plasma temperature contour $T \approx 50{,}000$ K gives a sufficiently reliable estimate for the heliopause location for the present purpose. The black lines in Figure 2 show the projection of the ISMF lines into the plane $\theta = 54°$, and color coding is used to show a total amplitude of ISMF, including the magnetic field component perpendicular to the plane $\theta = 54°$. The perpendicular component of magnetic field, however, is negligible in Figure 2 except a tiny region near the heliopause around (x, y) $\approx$ (129 au, 0 au). So ISMF in the azimuthal cut through $\theta = 54°$ is close to a two-dimensional magnetic field, which is nearly parallel to the plane $\theta = 54°$.

Figure 3 shows the 1.11 keV ENA fluxes at the Sun/*IBEX* location versus polar angle in the azimuthal cut through $\theta = 54°$ in which the peak flux is largest (see Figure 1). The red line in the left panel of Figure 3 shows the *IBEX* first five-year averaged ENA flux (McComas et al. 2014a), and the diffuse GDF separated from the *IBEX* first five-year averaged ENA flux (Schwadron et al. 2014) is shown by the black dashed line. The error bars show $\pm 3\sigma$, where σ is the standard deviation reported for the *IBEX* data. The right panel in Figure 3 shows a comparison between the *IBEX* and model fluxes. The data plotted "*IBEX*–GDF" are the observed "pure ribbon" flux, which is a difference between the *IBEX* and GDF fluxes shown in the left panel, and error bars show $\pm 3\sigma$ for the *IBEX* data. The four model profiles are shown for the four scenarios of energetic proton pitch angle scattering in the LISM; no diffusion (No Diff), diffusion due to the SSLT only, the LSIT only, and the composite LSIT & SSLT.

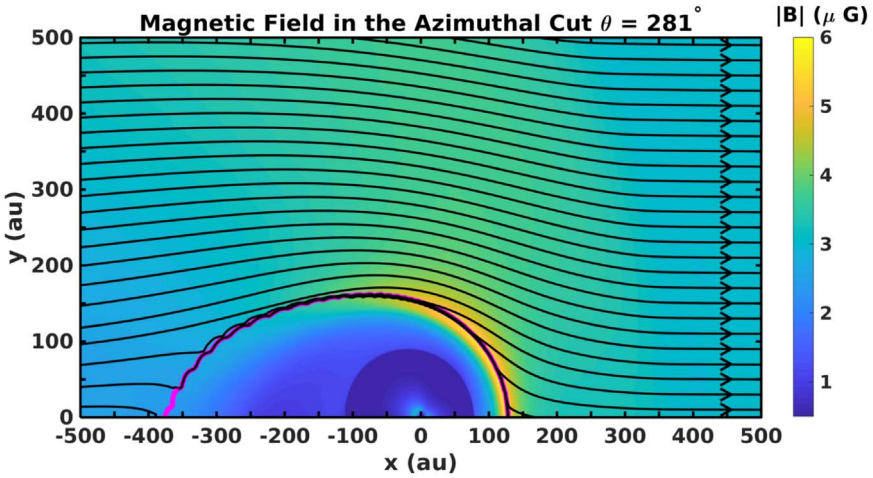

Figure 4. Same as in Figure 2, except for the azimuthal cut through $\theta = 281°$.

A full width at half maximum (FWHM) for the "*IBEX*–GDF" flux in the right panel of Figure 3 is estimated to be FWHM $\sim 17°-27°$. This estimate is close to the previously reported FWHM $\sim 15°-25°$ for a "pure ribbon" after the diffuse GDF is removed from the *IBEX* observations (e.g., Fuselier et al. 2009; Schwadron et al. 2014). Note that because *IBEX* has single-pixel $\sim 7° \times 7°$ sensors, the errors in angular resolution are at least a few degrees, and so we have to remember this fact in all the angular estimates presented here and below. The model cases "No Diff" and "SSLT" are close to each other because the SSLT does not scatter energetic protons with pitch angles close to 90° (see Paper I for more details). An FWHM for these two cases is $\sim 20°$, which is much larger than the respective FWHM in Paper I ($\sim 3°$). The FWHM $\sim 20°$ agrees well with the observed FWHM for a "pure ribbon." In two other model cases, "LSIT" and "LSIT & SSLT," the respective FWHMs are $\sim 24°$ and $\sim 20°$, which are also in the range of the observed ribbon FWHMs. So, in striking contrast to Paper I, the ribbon FWHMs obtained here are close to each other in all four scenarios of the energetic proton scattering. This means that we cannot discriminate between the shown model cases only on the basis of FWHMs of their flux profiles. Another conclusion that may be also drawn from the above results is the one that pitch angle scattering is not a major mechanism that controls ribbon width. Instead, the ribbon width is mainly controlled by draping of the ISMF around the HP because here we have FWHM $\sim 20°$ for the case "No Diff," whereas a simplified model for the ISMF in Paper I gives a much smaller FWHM $\sim 3°$ for the same model case.

The polar angles of peaks for all model profiles in the right panel of Figure 3 are $\sim 3°$ larger compared to the polar angle of peak in the "*IBEX*–GDF" flux. This discrepancy, however, may be relatively easily eliminated by slightly rotating the vector of pristine ISMF around the nose direction in our MHD-plasma/kinetic-neutral model of the heliosphere–LISM interaction. Doing so we can increase a polar angle of the *IBEX* flux peak in the polar coordinates centered on an updated direction of pristine ISMF. At the same time, Figure 2 will remain nearly the same, and so the polar angles of model peaks will also remain nearly the same. In addition, we can also decrease the peak polar angles in our model by simply reducing a strength of ISMF at infinity, since simulations by Heerikhuisen et al. (2014) show that the ribbon radius grows with increasing magnetic field strength. Also, the above misalignment of $\sim 3°$ in the flux peaks may be simply caused by a limited angular resolution of the *IBEX* fluxes as we noted above.

The "*IBEX*–GDF" flux profile in the right panel of Figure 3 is bracketed by the two model profiles "No Diff" and "LSIT," whereas the "LSIT & SSLT" model profile is well below the *IBEX* observations. (Note that a good agreement between the "*IBEX*–GDF" flux and all the model fluxes in the regions of small and large polar angles does not deserve much attention, because both the "*IBEX*–GDF" and model fluxes there are well below the GDF. So primary attention in comparing the model and *IBEX* fluxes should be given to the region around flux maximum.) So it is likely that generation of the SSLT in the azimuthal cut through $\theta = 54°$ is suppressed. On the other hand, an interplay of scenarios "No Diff" and "LSIT" can lead to a good agreement with observations. We have also to emphasize that an existence of the LSIT is firmly established by both the remote and in situ observations (see Paper I for more details). So we cannot assume above that case "No Diff" is actually the case "SSLT." Otherwise, it would imply that case "LSIT & SSLT" also exists. Our conclusion regarding suppression of the SSLT generation is strongly supported by previous theoretical works by Gamayunov et al. (2010, 2017) and Florinski et al. (2016), where the authors showed that distribution of energetic protons in the ribbon direction is likely to be stable with respect to a generation of the SSLT. This conclusion is also supported by the *Voyager 1* observations in the LISM (Burlaga et al. 2014). While those observations are taken in a different radial direction than the direction to the *IBEX* ribbon, they clearly show that the level of the observed SSLT does not exceed the noise level of the magnetometer on *Voyager 1*. Given all the facts listed in this paragraph, it is quite possible that the SSLT is not generated not only in the azimuthal cut $\theta = 54°$, but also in different directions in the LISM.

2.2. Azimuthal Cut through $\theta = 281°$

Figure 4 shows ISMF in the azimuthal cut through $\theta = 281°$. As in Figure 2, the magnetic field is obtained from our global MHD-plasma/kinetic-neutral model of the heliosphere–LISM interaction, and all the used notations are the same as above. The perpendicular component of magnetic field in Figure 4 is negligible, except a small region of ~ 50 au near the heliopause at $(x, y) \approx (128\text{ au}, 0\text{ au})$. So, similar to Figure 2, ISMF in the

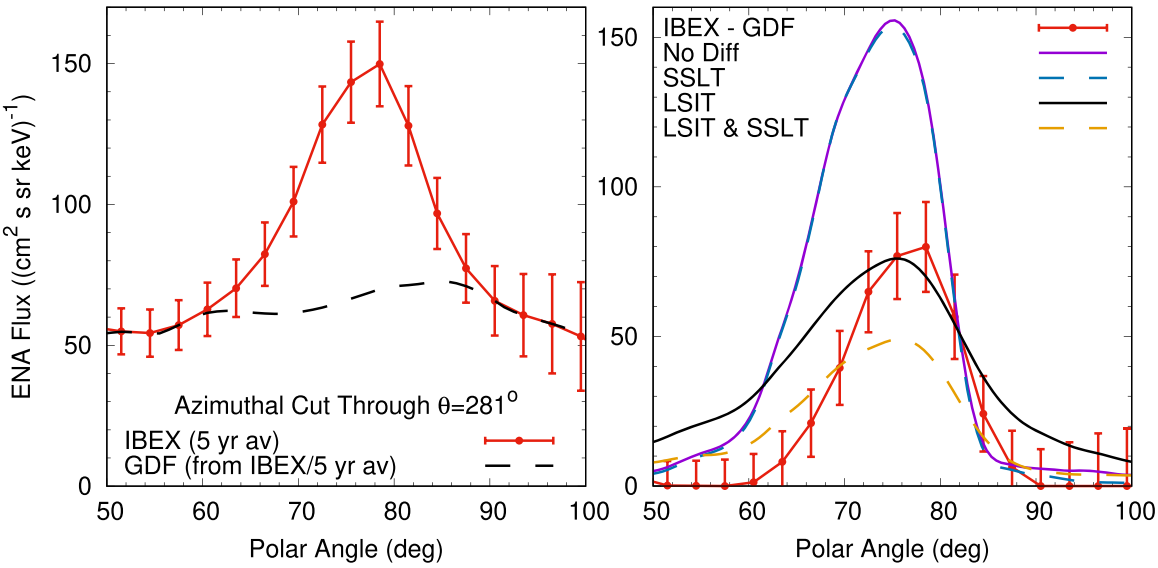

Figure 5. Same as in Figure 3, except for the azimuthal cut through $\theta = 281°$.

azimuthal cut through $\theta = 281°$ is also close to a two-dimensional magnetic field, which is nearly parallel to the plane $\theta = 281°$.

Figure 5, similar to Figure 3, shows the 1.11 keV ENA fluxes at the Sun/*IBEX* location versus polar angle, but in the azimuthal cut through $\theta = 281°$. The *IBEX* peak flux in the left panel of Figure 5 is 75% of the respective peak flux in Figure 3 (see also the right panel in Figure 1 for comparison). In agreement with this, the model peak fluxes in the right panel of Figure 5 also decrease (except the case "No Diff") compared to the respective peak fluxes in Figure 3. Despite the decrease, the separations between flux peaks in the model cases "LSIT" and "LSIT & SSLT" are nearly the same in both Figures 3 and 5. This suggests that the model "LSIT" and "LSIT & SSLT" flux peak separation is nearly the same in different azimuthal cuts through the ribbon.

An FWHM for the "*IBEX*–GDF" flux in the right panel of Figure 5 is FWHM $\sim 11°-19°$. On average this is smaller than the FWHM in the azimuthal cut $\theta = 54°$. An FWHM for the cases "No Diff" and "SSLT" is $\sim 15°$, which is in the range of the observed FWHMs for a "pure ribbon." In the two other cases, "LSIT" and "LSIT & SSLT," the respective FWHMs are $\sim 21°$ and $\sim 19°$. Taking into account an error $\sim 3°$ for the *IBEX* angular resolution, and so for the *IBEX* FWHMs estimated above, we have to conclude that all the model FWHMs are in the range of the observed FWHMs in the azimuthal cut through $\theta = 281°$. Similar to Figure 3, the ribbon FWHMs obtained here are also close to each other in all four scenarios of the energetic proton scattering. Consequently, the ribbon width in the azimuthal cut $\theta = 281°$ is also mainly controlled by draping of the ISMF around the HP, but not a pitch angle scattering of energetic protons in the LISM.

In the right panel of Figure 5, the polar angles of peaks in the model flux profiles are $\sim 2°$ smaller compared to the polar angle of peak in the "*IBEX*–GDF" flux. So the model peaks here are shifted in the opposite direction from the observed flux peak compared to those in Figure 3. This means that we cannot decrease a misalignment of the model and observed flux peaks in both Figures 3 and 5 by changing strength of the pristine ISMF in our global model. However, as we emphasized above, the discrepancies may be decreased in both azimuthal cuts by slightly rotating the vector of pristine ISMF around the nose direction in our MHD-plasma/kinetic-neutral model of the heliosphere–LISM interaction. (Note that the outlined procedure may be used in future works to refine a direction of the pristine ISMF in our global model by minimizing a total misalignment between the model and observed flux peaks in different azimuthal cuts.)

Finally, paying attention to the region around flux maximum in the right panel of Figure 5, we see that the "*IBEX*–GDF" flux agrees well with the model profile "LSIT," whereas the model profile "No Diff" is well above the *IBEX* observations, but the "LSIT & SSLT" model profile is well below the *IBEX* observations. So, similar to the azimuthal cut in Figure 3, it is likely that generation of the SSLT in the azimuthal cut through $\theta = 281°$ is also suppressed. In contrast to Figure 3, however, the scenario "No Diff" is not likely to take place in the azimuthal cut $\theta = 281°$, and only a pitch angle scattering by the LSIT takes place there.

3. Conclusions

This work follows up a recent numerical test by Gamayunov et al. (2017) that has strongly supported a "weak scattering" version of the secondary ENA model of the *IBEX* ribbon formation. Here we have extended the scope of the Gamayunov et al. model by using a more realistic ISMF from our global MHD-plasma/kinetic-neutral simulation of the heliosphere–LISM interaction instead of a simple analytical model used by Gamayunov et al. (2017). ISMF from the MHD-plasma/kinetic-neutral model has a more realistic magnetic field draping around the HP that qualitatively and quantitatively affects the previous results. Similar to the paper by Gamayunov et al. (2017), here we also have purposely turned off an ENA production in the IHS in order to focus solely on our model of ribbon. The model ribbon flux can then be compared directly to the ribbon flux observed by *IBEX* once the diffuse GDF has been subtracted out. The main conclusions of our work are summarized below.

1. A pitch angle scattering of energetic protons in the LISM is not a major mechanism that controls the width of *IBEX*

ribbon. Instead, the ribbon width is mainly controlled by draping of the ISMF around the HP.

2. An intensity of ribbon is strongly controlled by pitch angle scattering of energetic protons in the LISM. Comparison of the model and *IBEX* fluxes suggests that generation of the SSLT is suppressed in the LISM. On the other hand, the LSIT alone or an interplay of scenarios "No Diff" and "LSIT" lead to a good agreement between the model fluxes and the *IBEX* observations.

This paper is based on work supported by the National Aeronautics and Space Administration (NASA) under grant Nos. NNX14AP24G, 80NSSC18K1221, NNX16AG83G, and NNX14AJ53G. The authors acknowledge the use of *IBEX* ribbon-separated data (GDF) published online at http://ibex.swri.edu/ibexpublicdata/Data_Release_8/.

ORCID iDs

Konstantin V. Gamayunov https://orcid.org/0000-0002-8768-8527
Jacob Heerikhuisen https://orcid.org/0000-0001-7867-3633

References

Burlaga, L. F., Florinski, V., & Ness, N. F. 2015, ApJL, 804, L31
Burlaga, L. F., Ness, N. F., Florinski, V., & Heerikhuisen, J. 2014, ApJ, 792, 134
Florinski, V., Heerikhuisen, J., Niemiec, J., & Ernst, A. 2016, ApJ, 826, 197
Funsten, H. O., DeMajistre, R., Frisch, P. C., et al. 2013, ApJ, 776, 30
Fuselier, S. A., Allegrini, F., Funsten, H. O., et al. 2009, Sci, 326, 962
Gamayunov, K. V., Heerikhuisen, J., & Rassoul, H. 2017, ApJ, 845, 63
Gamayunov, K. V., Zhang, M., & Rassoul, H. 2010, ApJ, 725, 2251
Giacalone, J., & Jokipii, J. R. 2015, ApJL, 812, L9
Heerikhuisen, J., Florinski, V., & Zank, G. P. 2005, JGR, 111, A06110
Heerikhuisen, J., Gamayunov, K. V., Zirnstein, E. J., & Pogorelov, N. V. 2016, ApJ, 831, 137
Heerikhuisen, J., & Pogorelov, N. V. 2010, in ASP Conf. Ser. 429, Numerical Modeling of Space Plasma Flows, Astronum-2009, ed. N. V. Pogorelov, E. Audit, & G. P. Zank (San Francisco, CA: ASP), 227
Heerikhuisen, J., Pogorelov, N. V., Zank, G. P., et al. 2010, ApJL, 708, L126
Heerikhuisen, J., Zirnstein, E. J., Funsten, H. O., Pogorelov, N. V., & Zank, G. P. 2014, ApJ, 784, 73
Isenberg, P. A. 2014, ApJ, 787, 76
McComas, D. J., Allegrini, F., Bochsler, P., et al. 2009, Sci, 326, 959
McComas, D. J., Allegrini, F., Bzowski, M., et al. 2014a, ApJS, 213, 20
McComas, D. J., Bzowski, M., Frisch, P., et al. 2010, JGR, 115, A09113
McComas, D. J., Bzowski, M., Frisch, P., et al. 2015, ApJ, 801, 28
McComas, D. J., Dayeh, M. A., Funsten, H. O., et al. 2011, JGR, 116, A02211
McComas, D. J., Lewis, W. S., & Schwadron, N. A. 2014b, RvGeo, 52, 118
McComas, D. J., Zirnstein, E. J., Bzowski, M., et al. 2017, ApJS, 229, 41
Pogorelov, N. V., Zank, G. P., & Ogino, T. 2004, ApJ, 614, 1007
Schwadron, N. A., & McComas, D. J. 2013, ApJ, 764, 92
Schwadron, N. A., Moebius, E., Fuselier, S. A., et al. 2014, ApJS, 215, 13
Zirnstein, E. J., Heerikhuisen, J., Funsten, H. O., et al. 2016, ApJL, 818, L18